

Compliant yet Brittle Mechanical Behavior of Li₂S-P₂S₅ Lithium-ion Conducting Solid Electrolyte

Frank P. McGrogan¹, Tushar Swamy², Sean R. Bishop^{1,3}, Erica Eggleton¹, Lukas Porz^{1,5}, Xinwei Chen^{1,6}, Yet-Ming Chiang¹, Krystyn J. Van Vliet^{1,4,}*

Departments of ¹Materials Science & Engineering, ²Mechanical Engineering, ³Nuclear Science and Engineering, and ⁴Biological Engineering, Massachusetts Institute of Technology, Cambridge, MA 02139 USA

⁵Institute of Materials Science, Technische Universität Darmstadt, Darmstadt 64287, Germany

⁶Current affiliation: Institute of Materials Research and Engineering, Singapore 138634

*Corresponding author: krystyn@mit.edu

Keywords: solid electrolytes, sulfides, Li-ion conductors, fracture toughness, mechanical properties

Abstract: Young's modulus, hardness, and fracture toughness are measured by instrumented nanoindentation for amorphous Li₂S – P₂S₅ Li-ion solid electrolyte. Although low modulus suggests good ability to accommodate chemomechanical strain, highly brittle behavior can lead to disruptive crack formation.

Li-ion batteries have provided compact, lightweight rechargeable energy storage enabling a range of new technologies over more than two decades. Recently, the drive towards both safer and higher energy density storage has motivated an increasing focus on all-solid-state batteries, wherein the solid electrolyte is anticipated to preclude dendrite formation leading to electrical shorting and is furthermore non-flammable. If realized, these advantages could significantly improve battery safety and enable use of higher energy density electrodes.^[1,2]

Crystalline and amorphous sulfide electrolytes (e.g., $\text{Li}_2\text{S-P}_2\text{S}_5$ or LPS) have now been widely reported to have Li-ion conductivity near room temperature that is high enough ($>10^{-4}$ S/cm) to warrant consideration as the basis for a new class of solid state batteries.^[3-5] A key concern in these and other solid electrolytes, however, is their mechanical stability in the presence of strains in the adjacent electrode materials accompanying reversible Li storage (intercalation or alloying) that may vary from a few percent by volume up to a factor of three (e.g., in the case of silicon anodes).^[6,7] Sulfide-based electrolytes have remarkably lower Young's modulus (~ 20 GPa^[8]) than many of these active materials (e.g., 100-200 GPa), as well as oxide-based solid electrolytes such as the garnets (100-200 GPa for $\text{Li}_7\text{La}_3\text{Zr}_2\text{O}_{12}$ or LLZO and $\text{Li}_{0.33}\text{La}_{0.57}\text{TiO}_3$ or LLTO^[8-10]), which initially suggested to us that the sulfides might exhibit superior strain-accommodation characteristics in solid state batteries. However, detailed understanding of elastoplastic and fracture properties, which has heretofore been lacking, is required to draw clear conclusions of material design and selection for sulfide solid electrolytes.

Here we used instrumented indentation to quantify three fundamental mechanical properties of an amorphous $\text{Li}_2\text{S-P}_2\text{S}_5$ (70:30 mol%) solid electrolyte prepared by a melt-quenching procedure: Young's elastic modulus E , hardness H , and fracture toughness K_{Ic} . Mechanical property characterization of the sulfide electrolytes is exceptionally challenging due to their extreme moisture sensitivity; exposure to air alone quickly degrades the sample surfaces. Therefore, we obtained E and H from instrumented indentation measurements within a specialized fluid cell that immersed the sample in mineral oil, a liquid medium that we found to be nonreactive with the

sulfide electrolyte (**Figure 1**). We evaluated K_{Ic} via post-indentation imaging of crack dimensions^[11,12] through a protective mineral oil film. These measurements provide an improved understanding of sulfide electrolyte mechanical properties necessary for predictive modeling of elastic stress distributions and fracture conditions in solid state battery structures.

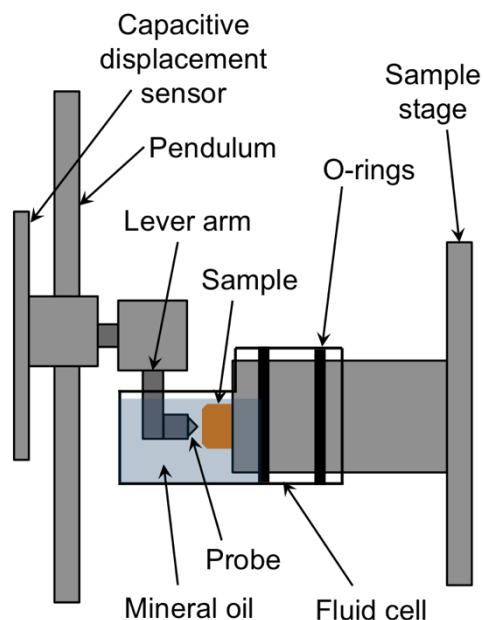


Figure 1. Schematic of liquid cell used to immerse the sulfide sample in mineral oil during instrumented indentation.

The elastic modulus E and hardness H of amorphous LPS were measured to be 18.5 ± 0.9 GPa and 1.9 ± 0.2 GPa, respectively. The E of LPS is thus much lower than that reported for typical oxide glasses; for example, soda-lime and borosilicate glasses have E of ~ 70 GPa.^[13] This relatively low E also corresponds to a shear modulus of $G = 7.1 \pm 0.3$ GPa (assuming elastic isotropy and Poisson's ratio $\nu = 0.3$ as reported by Sakuda et al.^[8]) that is sufficiently compliant to allow dendritic penetration by the Monroe and Newman criterion.^[14] The hardness H is at the low end of the range for oxide glasses, which vary from 2 to 8 GPa,^[15] and at the high end of reported hardnesses for chalcogenide glasses, which range from 0.3 GPa to 2 GPa.^[15] Note that the hardness of LPS is similar to that of crystalline metallic alloys (e.g., aluminum 7075^[16]) but about three orders of magnitude higher than that of pure alkali metals.^[17]

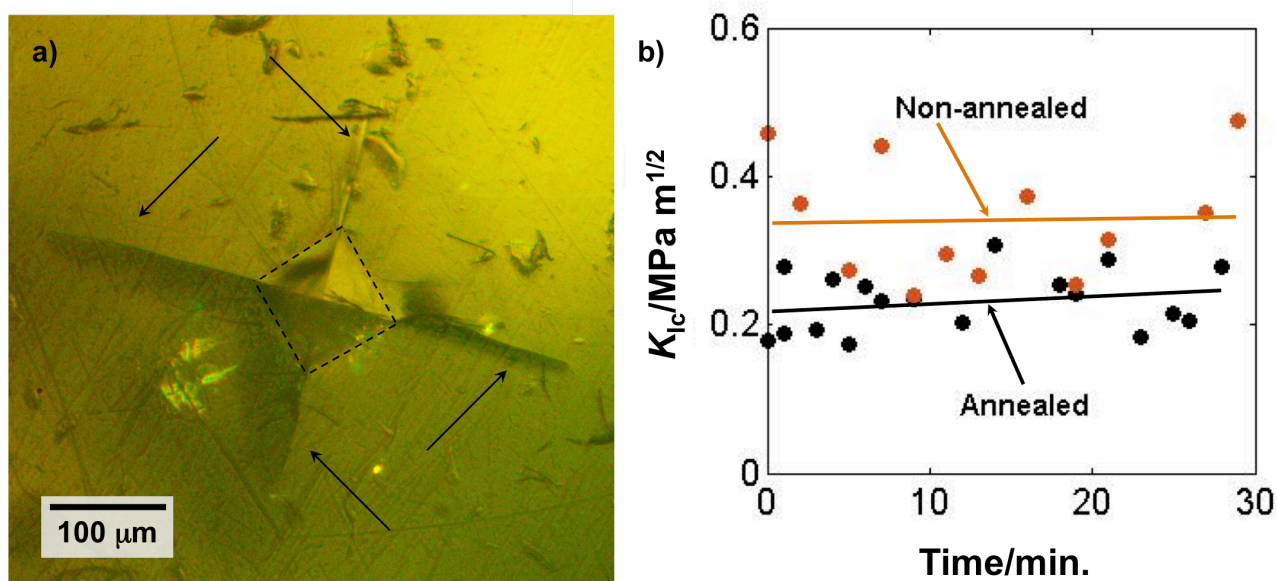


Figure 2. (a) Fracture in the form of visible cracks (arrows) resulting from Vickers indentation (dashed diamond) load of ~ 10 N on glassy Li₂S-P₂S₅ (LPS). (b) K_{Ic} did not change detectably or steadily with time, for either the annealed or non-annealed samples, indicating stability of the LPS surface under mineral oil.

Fracture toughness K_{Ic} as measured by crack length analysis (**Figure 2a**) was 0.23 ± 0.04 MPa m^{1/2}, more than a factor of two lower than oxide glasses such as soda-lime and borosilicate glasses, which exhibit K_{Ic} values in the range of $0.5 - 1.0$ MPa m^{1/2}.^[18] As discussed in the Experimental Section, an annealing step that heated the sample to slightly below the glass transition temperature was included to consider whether residual stresses from quenching significantly affected K_{Ic} . A second sample prepared without this annealing step was tested for comparison. The measured K_{Ic} of the non-annealed sample was 0.34 ± 0.08 MPa m^{1/2}, which was significantly higher than that measured for the annealed sample ($p < 0.001$, Welch's t -test). This statistically significant difference was modest (0.11 MPa m^{1/2}) and within a range that could be attributed to sample-to-sample variation, and thus this comparison demonstrates chiefly that annealing at 150°C did not increase the effective K_{Ic} by relieving thermal stresses. K_{Ic} did not vary detectably as a function of time over the experimental duration (**Figure 2b**), indicating that the sample surface was chemically stable under mineral oil for these durations.

Note that the relatively low K_{Ic} measured for this solid electrolyte was comparable to that for delithiated Li_xCoO_2 cathode; upon delithiation, K_{Ic} of Li_xCoO_2 decreases from 0.94 to 0.25 $MPa\ m^{1/2}$, as we have reported previously.^[19] As the data presented here are the first report of plastic and fracture properties of any sulfide solid electrolytes, these magnitudes provide a key baseline to test whether substantial variations exist in the LPS family as a function of composition or crystallinity. Thus, overall this solid electrolyte is elastically compliant with relatively low resistance to reversible deformation, while also brittle with low resistance to fracture. In comparison to LPS, solid polymer electrolytes are significantly more compliant ($E \sim 1\ MPa$ ^[20,21] to $E \sim 1\ GPa$ ^[22]) with typically higher fracture toughness ($K_{Ic} \sim 0.5\ MPa\ m^{1/2}$).^[22] Solid electrolyte garnet-type oxides such as LLTO and LLZO are much stiffer ($E \sim 100\ GPa$), but likewise less brittle ($K_{Ic} \sim 0.9$ to $1.6\ MPa\ m^{1/2}$ when measured via Newton-scale indentation as reported herein).^[10,23]

To confirm the structure and conductivity of the sample, we ground the LPS to a powder form and conducted X-ray diffraction (XRD) and electrochemical impedance spectroscopy (EIS) measurements. **Figure 3a** shows the XRD pattern of the melt-quenched LPS sample (after grinding to powder), the same material after annealing for stress-relief, and the pattern reported by Minami et al.^[24] for “glassy” LPS powder obtained via the same melt-quench process. We observed broad peaks for the present samples indicating a high degree of disorder; the extent of short-range order or possibly nanocrystalline content requires more detailed study, such as by pair-distribution function analysis. Direct observation by transmission electron microscopy and related methods is challenged by the extreme moisture sensitivity of these materials. However, as discussed below, the ionic conductivity of the present material is comparable to those reported previously for other LPS considered to be amorphous; specifically, the conductivity was reported to be somewhat lower for amorphous than for crystalline LPS,^[24] and thus our samples are assumed to be similarly disordered.

Figure 3b shows EIS results from experiments conducted with SS blocking electrodes (SS/LPS/SS, as shown in the inset) on the as-synthesized LPS powder, and after annealing at

150°C for 5 h. The reproducible XRD and impedance spectra after annealing indicates that no further change in the structure occurred during this stress relaxation step. The intercept with the horizontal axis at high frequency, indicated by the arrow in Figure 3b, is attributed to the bulk electrolyte resistance. Upon converting resistance to conductivity by accounting for the geometry of the sample, we obtain a room-temperature conductivity value of $\sim 3 \times 10^{-4}$ S/cm for the as-synthesized LPS powder. This magnitude is consistent with other reports in the literature for amorphous LPS.^[24] Figure 3b shows that the conductivity was unchanged by annealing.

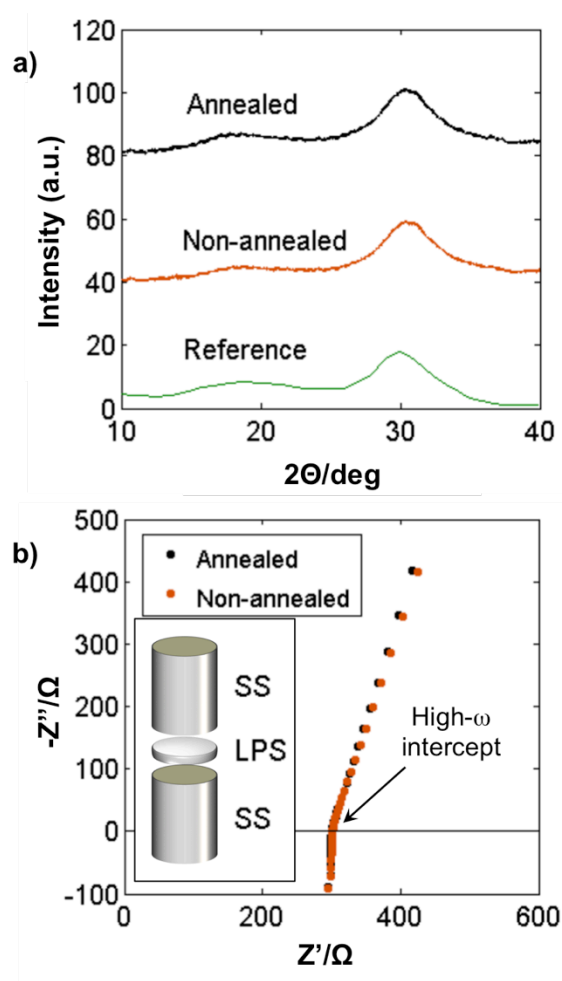


Figure 3. Characterization of $\text{Li}_2\text{S}-\text{P}_2\text{S}_5$ (LPS). (a) X-ray diffraction pattern of the as-synthesized LPS powder, after annealing at 150°C for 5 h, and reference pattern reproduced from Minami et al.^[24] Absence of sharp peaks suggests a predominantly glassy or amorphous phase. (b) Ionic conductivity data measured via EIS for SS/LPS/SS configuration in inset, where SS denotes stainless steel.

To summarize the variation in mechanical properties that would typically be present in an all-solid-state lithium battery, we illustrate in **Figure 4** a simplified battery “stack” consisting of a Li_xCoO_2 cathode, LPS electrolyte, and Li metal anode, along with the corresponding E , H , and K_{Ic} . During cycling over typical capacity limits, Li_xCoO_2 is known to undergo $\sim 1.9\%$ molar volume change,^[19,25] while the lithium electrode will undergo an absolute volume change dictated by the amount of Li being reversibly transported. The relatively low E of LPS indicates that imposed strain, such as those incurred by cyclic expansion of an adjacent electrode, will be accommodated with relatively less stress than a high modulus electrolyte such as a garnet. However, the low K_{Ic} of LPS also means that brittle fracture could occur at lower stresses, depending on details of defect size and population. Note that even for this simplified stack, additional information such as the interfacial mechanical properties and defect population are necessary to predict modes of failure. However, the present results are a significant step towards understanding, modeling, and designing all-solid-state batteries for electro-chemo-mechanical reliability.

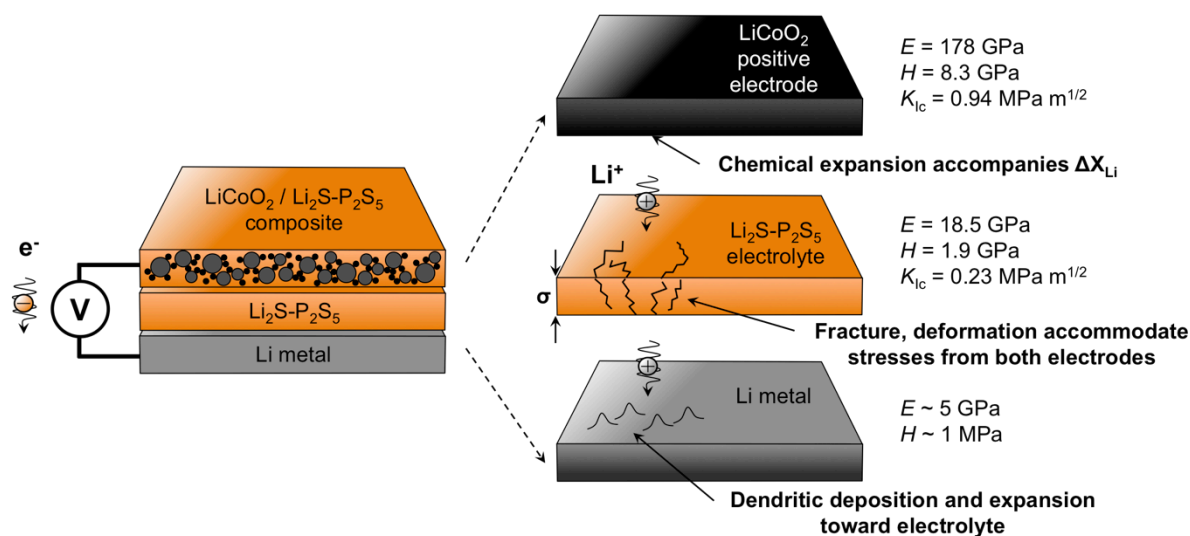


Figure 4. Summary of $\text{Li}_2\text{S-P}_2\text{S}_5$ (LPS) mechanical property data in the context of the all solid-state battery. While relatively low stiffness would enable strain accommodation from a composite Li_xCoO_2 cathode, low fracture toughness indicates high susceptibility to fracture and passage of Li dendrites. Data for Li_xCoO_2 is taken from Swallow et al.^[19] and E and H Li estimates are based on Samsonov,^[17] fracture toughness of Li is not reported to our knowledge.

In conclusion, we determined the Young's modulus, hardness, and fracture toughness of glassy $\text{Li}_2\text{S-P}_2\text{S}_5$ solid electrolyte of 70:30 composition to be 18.5 ± 0.9 GPa, 1.9 ± 0.2 GPa, and 0.23 ± 0.04 $\text{MPa m}^{1/2}$, respectively, via indentation-based methods that maximized phase stability of the LPS sample. These results show that this LPS material – and by inference other solid electrolytes in the solid sulfide family – are distinguished as compliant yet significantly more brittle than crystalline oxide electrolytes considered for the same applications. Although the low stiffness of LPS suggests a capability of this solid electrolyte material to accommodate elastic mismatch with adjacent phases such as storage electrodes and current collectors in a solid state battery, this capability is compromised by the low fracture toughness and corresponding high sensitivity to preexisting or cycling-generated flaws.

Experimental Section

Sample preparation: Li_2S (Alfa Aesar, 99.9%) and P_2S_5 (Sigma Aldrich, 99%) were mixed at a ratio of 70/30 mol% in an argon-filled glovebox, and placed inside a carbon coated quartz ampoule which was then sealed under house vacuum. The sealed ampoule was placed in a preheated furnace at 750°C for 2 h, followed by quenching in ice water to obtain the glassy LPS solid electrolyte. To remove thermal stresses that could affect the measurements, the quenched sample was annealed at 150°C for 5 hours, well below the glass transition temperature of $\sim 220^\circ\text{C}$.^[26]

To obtain polished samples for mechanical characterization, the solid sample of mm-scale thickness was mounted to a stainless steel spacer (via low-viscosity cyanoacrylate) within an argon-filled glovebox and attached to a hand-operated polishing tool. The sample was then polished in the glovebox using silicon carbide sandpaper of decreasing grit size (120, 500, 800, 1200, 2400, and 4000) and diamond polishing pads ($3\ \mu\text{m}$, $1\ \mu\text{m}$, and $0.5\ \mu\text{m}$; UltraPrep, Beuhler

Limited, Lake Bluff, IL). Tetrahydrofuran (anhydrous, Sigma-Aldrich, > 99.9% purity) was used to rinse the sample and polishing tool after each polishing step, as it was observed to be non-reactive with the sample and other experimental components.

The LPS powder for conductivity samples and X-ray diffraction (XRD) measurements was obtained by first manually grinding a quenched/annealed solid sample, and then ball milling for 100 min in a SPEX SamplePrep® Mixer/Mill 8000 M.

Phase and Electrochemical Characterization: The XRD pattern of the as-synthesized LPS solid electrolyte powder was obtained using a PANalytical X'Pert Pro multipurpose diffractometer equipped with a Cu-K α radiation source and an X'Celerator detector. The LPS powder was cold-pressed in a 1.3 cm polycarbonate tube at 360 MPa between two stainless steel (SS) current collectors to a thickness of ~1 mm, preparing an SS/LPS/SS cell. Electrochemical impedance spectroscopy (EIS) measurements were conducted at room temperature using a Solartron 1400/1470E cell test system, wherein the sinusoidal voltage amplitude was set to 10 mV and the frequency was swept from 1 MHz to 1 Hz.

Mechanical Characterization: To measure E and H via instrumented indentation, flat and polished LPS samples were mounted within a fluid cell designed specifically for use in a commercial, instrumented indenter (MicroMaterials, LLC, Wrexham, UK), as shown in Figure 1, and filled with mineral oil (Alfa Aesar). In this design, a lever arm is attached to the indentation pendulum and submerged in the liquid cell, so that all measurements take place with the sample and indenter immersed fully in the liquid medium.^[27,28] Calibrations of frame compliance were conducted using the instrument software to account for any additional frame compliance (i.e., displacement of the instrument itself under applied load to the sample) that was introduced by the lever arm.

To ensure that the sample was not exposed to air (specifically, moisture) during the entire mounting and measurement process, the sample mounting was conducted in an argon-filled glovebox (less than 10 ppm H₂O and 1 ppm O₂), and the liquid cell was filled with mineral oil

therein. The liquid cell was then transferred from the glovebox to the instrumented indenter, and carefully mounted in the instrument to maintain full sample immersion. The sample did not exhibit any visible changes in color or opacity throughout the indentation experiment, which is in stark contrast to a surface reaction forming a white crust on the sulfide that is otherwise observed upon < 5 min of exposure to ambient air. (Gas purging to produce dry environments within the testing chamber were less successful in preserving sample surface integrity over the experiment durations, due to the high moisture sensitivity of such materials.)

Mechanical properties E and H were measured at 39 distinct sample surface locations ($n = 39$ indentations, comprising a rectangular grid of 4×10 replicate load-displacement profiles with one fiduciary marker in the corner of the grid) in this liquid cell configuration. A diamond probe of cube-corner geometry was used with load-depth hystereses acquired up to a maximum load of 20 mN, resulting in maximum depths that were $\sim 2 \mu\text{m}$ and thus approximately three orders of magnitude less than the mm-scale sample thickness, such that finite-thickness effects were reasonably neglected. Data were acquired over a period of 120 s loading and 30 s unloading, with an intermediate dwell time at maximum load of 10 s. Center-to-center spacing of the indentations was $70 \mu\text{m}$. Since indentation depths were typically $\sim 2 \mu\text{m}$, and therefore well beyond the probe apex, an ideal cube corner area function was used for subsequent data analysis.

From the load-depth hystereses, reduced elastic moduli E_r were calculated using Equation 1,^[29,30] wherein dP/dh represents the initial elastic response upon unloading:

$$E_r = \frac{\sqrt{\pi}}{2} \frac{1}{\sqrt{A}} \frac{dP}{dh} \quad (1)$$

and P , h , and A correspond to the measured load, measured displacement, and calculated projected indentation area, respectively. The material Young's modulus E was calculated from E_r by accounting for the elastic properties of the diamond indenter,^[31] as shown in Equation 2:

$$E = \frac{1 - \nu^2}{\frac{1}{E_r} - \frac{1 - \nu_i^2}{E_i}} \quad (2)$$

where E_i and Poisson's ratio ν_i of the diamond indenter were taken to be 1070 GPa and 0.07, respectively; Poisson's ratio ν of the sample was assumed as 0.3, as experimentally determined by Sakuda et al.^[8] Hardness H was calculated as in Equation 3, where A is the projected indentation area and P_{\max} is the maximum applied load:

$$H = \frac{P_{\max}}{A} \quad (3)$$

Fracture toughness K_{Ic} can be quantified for brittle materials, including solid Li-intercalating electrodes, via direct measurement of sudden displacement excursions or “pop-ins” extending several nanometers during instrumented indentation.^[19,32,33] However, these LPS solid electrolyte samples did not exhibit detectable displacement excursions associated with radial cracking under our accessible instrumented indentation conditions. Thus, we conducted microindentation with a diamond Vickers probe geometry (LECO LM248AT; Saint Joseph, MI) to apply Newton-scale loads to the material. The sample was not immersed within oil during such experiments due to instrument constraints. However, the surfaces of samples removed from mineral oil baths immediately before testing retained an oil surface film and thus remained stable for 15-30 minutes as required for these experiments. Beyond such durations, visible oxidation reaction products were apparent in some surface regions. Indentations were conducted only on pristine regions of the surface, and optical images were acquired through the oil film immediately before and after the indentations. Applied load of 1000 gf (9.8 N) with the Vickers probe using a dwell time of 15 s regularly resulted in the formation of radial cracks, typically from all four corners of the indentation, as shown in Figure 2a. Replicate data were collected on a quenched/annealed LPS

sample ($n = 18$ measurements) and on a quenched/non-annealed LPS sample ($n = 12$) to investigate the possible effects of residual thermal stress on the measurement.

Estimation of K_{Ic} from radial cracks uses the crack length c , measured optically from the center of the indentation to the crack tip. Taking E and H as the values determined by the prior instrumented indentation experiments, K_{Ic} was calculated by Equation 4:

$$K_{Ic} = k \left(\frac{E}{H} \right)^{1/2} \frac{P}{c^{3/2}} \quad (4)$$

where P is the applied load equal to 9.81 N and k is a constant taken to be 0.016 for the Vickers probe geometry.^[12] We note that this approach provides a measure of K_{Ic} that is accessible to small sample geometries which, though quantified thus and reported for other brittle materials, is best considered as an approximation of the plane strain, Mode I tensile fracture toughness.

All mechanical property data are reported as mean +/- standard deviation. For comparing means obtained with different variances and sample sizes n , Welch's t -test was used to identify differences with statistical significance.

Acknowledgements

We gratefully acknowledge support from the US Department of Energy's Office of Basic Energy Science for the Chemomechanics of Far-From-Equilibrium Interfaces (COFFEI) small group, through award number DE-SC0002633 (J. Vetrano, Program Manager). This work made use of the DMSE Metlab (Laboratory for Physical Metallurgy) at MIT (Meri Treska, Senior Lecturer). We also acknowledge use of the MIT Nanomechanical Technology Laboratory (A. Schwartzman, Manager).

Received: ((will be filled in by the editorial staff))

Revised: ((will be filled in by the editorial staff))

Published online: ((will be filled in by the editorial staff))

References

- [1] K. Takada, *Acta Mater.* **2013**, *61*, 759.
- [2] J. Li, C. Ma, M. Chi, C. Liang, N. J. Dudney, *Adv. Energy Mater.* **2015**, *5*, 1401408.

- [3] N. Kamaya, K. Homma, Y. Yamakawa, M. Hirayama, R. Kanno, M. Yonemura, T. Kamiyama, Y. Kato, S. Hama, K. Kawamoto, A. Mitsui, *Nat. Mater.* **2011**, *10*, 682.
- [4] Z. Liu, W. Fu, E. A. Payzant, X. Yu, Z. Wu, N. J. Dudney, J. Kiggans, K. Hong, A. J. Rondinone, C. Liang, *J. Am. Chem. Soc.* **2013**, *135*, 975.
- [5] Y. Seino, T. Ota, K. Takada, A. Hayashi, M. Tatsumisago, *Energy Environ. Sci.* **2014**, *7*, 627.
- [6] W. H. Woodford, W. C. Carter, Y.-M. Chiang, *Energy Environ. Sci.* **2012**, *5*, 8014.
- [7] S. R. Bishop, D. Marrocchelli, C. Chatzichristodoulou, N. H. Perry, M. B. Mogensen, H. L. Tuller, E. D. Wachsman, *Annu. Rev. Mater. Res.* **2014**, *44*, 205.
- [8] A. Sakuda, A. Hayashi, Y. Takigawa, K. Higashi, M. Tatsumisago, *J. Ceram. Soc. Japan* **2013**, *121*, 946.
- [9] S. Yu, R. D. Schmidt, R. Garcia-Mendez, E. Herbert, N. J. Dudney, J. B. Wolfenstine, J. Sakamoto, D. J. Siegel, *Chem. Mater.* **2016**, *28*, 197.
- [10] Y.-H. Cho, J. Wolfenstine, E. Rangasamy, H. Kim, H. Choe, J. Sakamoto, *J. Mater. Sci.* **2012**, *47*, 5970.
- [11] D. S. Harding, W. C. Oliver, G. M. Pharr, *Mat. Res. Soc. Symp. Proc.* **1995**, *356*, 663.
- [12] G. R. Anstis, P. Chantikul, B. R. Lawn, D. B. Marshall, *J. Am. Ceram. Soc.* **1981**, *64*, 533.
- [13] *Materials Data Book*, Cambridge University Engineering Department, Cambridge, UK, **2003**.
- [14] C. Monroe, J. Newman, *J. Electrochem. Soc.* **2005**, *152*, A396.
- [15] J. E. Shelby, *Introduction to Glass Science and Technology*, Royal Society Of Chemistry, **2005**.
- [16] T. A. Venkatesh, K. J. Van Vliet, A. E. Giannakopoulos, S. Suresh, *Scr. Mater.* **2000**, *42*, 833.
- [17] G. V Samsonov, in *Handb. Physicochem. Prop. Elem.* (Ed.: G. V Samsonov), Springer US, **1968**, pp. 387–446.
- [18] K. K. Ray, A. K. Dutta, *Br. Ceram. Trans.* **1999**, *98*, 165.
- [19] J. G. Swallow, W. H. Woodford, F. P. McGrogan, N. Ferralis, Y.-M. Chiang, K. J. Van Vliet, *J. Electrochem. Soc.* **2014**, *161*, F3084.
- [20] D. R. MacFarlane, J. Sun, P. Meakin, P. Fasouloupoulos, J. Hey, M. Forsyth, *Electrochim. Acta* **1995**, *40*, 2131.
- [21] S. Ramesh, T. Winie, A. K. Arof, *Eur. Polym. J.* **2007**, *43*, 1963.

- [22] D. H. Builes, J. P. Hernandez-Ortiz, M. A. Corcuera, I. Mondragon, A. Tercjak, *ACS Appl. Mater. Interfaces* **2014**, *6*, 1073.
- [23] J. Wolfenstine, H. Jo, Y.-H. Cho, I. N. David, P. Askeland, E. D. Case, H. Kim, H. Choe, J. Sakamoto, *Mater. Lett.* **2013**, *96*, 117.
- [24] K. Minami, A. Hayashi, M. Tatsumisago, *J. Ceram. Soc. Japan* **2010**, *118*, 305.
- [25] J. N. Reimers, J. R. Dahn, *J. Electrochem. Soc.* **1992**, *139*, 2091.
- [26] K. Minami, F. Mizuno, A. Hayashi, M. Tatsumisago, *Solid State Ionics* **2007**, *178*, 837.
- [27] G. Constantinides, Z. I. Kalcioğlu, M. McFarland, J. F. Smith, K. J. Van Vliet, *J. Biomech.* **2008**, *41*, 3285.
- [28] B. Qing, K. J. Van Vliet, *Mol. Syst. Des. Eng.* **2016**, *1*, 290.
- [29] W. C. Oliver, G. M. Pharr, *J. Mater. Res.* **1992**, *7*, 1564.
- [30] W. C. Oliver, G. M. Pharr, *J. Mater. Res.* **2004**, *19*, 3.
- [31] A. C. Fischer-Cripps, *Nanoindentation*, Springer New York, New York, NY, **2002**.
- [32] J. S. Field, M. V Swain, R. D. Dukino, *J. Mater. Res.* **2003**, *18*, 1412.
- [33] M. Qu, W. H. Woodford, J. M. Maloney, W. C. Carter, Y.-M. Chiang, K. J. Van Vliet, *Adv. Energy Mater.* **2012**, *2*, 940.

Figure Captions

Figure 1. Schematic of liquid cell used to immerse the sulfide sample in mineral oil during instrumented indentation.

Figure 2. (a) Fracture in the form of visible cracks (arrows) resulting from Vickers indentation (dashed diamond) load of ~10 N on glassy $\text{Li}_2\text{S-P}_2\text{S}_5$ (LPS); (b) K_{Ic} did not change detectably or steadily with time, for either the annealed or non-annealed samples, indicating stability of the LPS surface under mineral oil.

Figure 3. Characterization of $\text{Li}_2\text{S-P}_2\text{S}_5$ (LPS). (a) X-ray diffraction pattern of the as-synthesized LPS powder, after annealing at 150°C for 5 h, and reference pattern reproduced from Minami et al.^[24] Absence of sharp peaks suggests a predominantly glassy or amorphous phase. (b) Ionic conductivity data measured via EIS for SS/LPS/SS configuration in inset, where SS denotes stainless steel.

Figure 4. Summary of $\text{Li}_2\text{S-P}_2\text{S}_5$ (LPS) mechanical property data in the context of the all solid-state battery. While relatively low stiffness would enable strain accommodation from a composite Li_xCoO_2 cathode, low fracture toughness indicates high susceptibility to fracture and passage of Li dendrites. Data for Li_xCoO_2 is taken from Swallow et al.^[19] and E and H Li estimates are based on Samsonov,^[17] fracture toughness of Li is not reported to our knowledge.